International Journal of Optomechatronics, 2: 75–87, 2008

ISSN: 1559-9612 print/1559-9620 online
DOI: 10.1080/15599610802081779

Taylor & Francis
Taylor & Francis Group

DESIGN OF A MEMS TUNABLE POLYMER GRATING FOR SINGLE DETECTOR SPECTROSCOPY

Steven Chin Truxal,[1] Katsuo Kurabayashi,[1,2] and Yi-Chung Tung[3]

[1]*University of Michigan Mechanical Engineering, Ann Arbor, Michigan, USA*
[2]*University of Michigan Electrical Engineering and Computer Science, Ann Arbor, Michigan, USA*
[3]*University of Michigan Biomedical Engineering, Ann Arbor, Michigan, USA*

High-speed, highly sensitive, miniature photospectroscopy techniques suited for a microfluidic platform enable rapid, cost-effective and efficient assays for numerous applications. Guided by these application requirements, we designed and demonstrated an innovative tunable diffraction grating implemented for spectroscopic measurements requiring minimal optics and signal processing. The device includes a flexible polymer microbridge with a nanoimprinted grating pattern on the top surface. Microelectromechanical system (MEMS) silicon actuators mechanically strain the microbridge to variably tune the grating period. Our innovative nanophotonic technology incorporating the tunable grating may guide future advancements of wavelength-discriminating detection for the identification and quantification of chemical and biological species.

Keywords: Comb drive; Grating; MEMS; PDMS; Polymer; Spectroscopy; Strain; Tunable

1. INTRODUCTION

Novel and innovative optical techniques and technologies provide the critical basis for expansion of scientific knowledge in modern life sciences and biotechnology. Emerging improvements in the fields of wavelength-discriminating optical detection are important and necessary in the identification and quantification of chemical and biological species based on photospectroscopy. Of particular relevance to lab-on-a-chip technology are monolithically integrated optical components that allow stand-alone microfluidic fluorescence spectroscopy without using an off-chip microscope.

Previous studies demonstrated key components for a MEMS-based miniaturized spectrometer, which can be, in principle, integrated in a microfluidic system. For example, Goldman et al. (1990) demonstrated a miniaturized planar waveguide spectrometer for chemical analysis. Their device consists of a waveguide deposited on a glass substrate with an etched grating, where collected light travels through the waveguide while interacting with chemical samples. The resulting spectra are dispersed depending on their wavelengths at the grating and analyzed using an array of photodiodes. Combining silicon micromachining and optical fiber technology,

Address correspondence to Steven Chin Truxal, University of Michigan Mechanical Engineering, 2350 Hayward St., Ann Arbor, MI 48109, USA. E-mail: trux@umich.edu

NOMENCLATURE

a	grating spatial period	V	voltage
a'	elongated grating period	$\Delta\lambda$	minimum detectable change in wavelength
D	Rayleigh distance	ε	engineering strain
F	force generated from actuator	ε_o	permittivity of free space, 8.854e-12 F/m
g	gap between comb electrodes	η_1	first order grating efficiency
m	order of diffraction	θ_1	first order angle of diffraction
N	number of grating grooves	λ	wavelength
N_g	number of comb drive electrode gaps	λ'	elongated incident wavelength
R	spectral resolving power	ν_1	nondimensional grating parameter
t	in-depth thickness of comb drive	ξ_1	nondimensional grating parameter

Mohr et al. (1991) developed another type of planar waveguide miniature spectrometer. This device introduces detected light into a polymer waveguide through an optical fiber and disperses it at a reflection grating, which has been fabricated using deep reactive ion etch. A similar approach was implemented for the device by Sander and Muller (2001), where a SiON layer was utilized as the waveguide. Yee et al. (1997) combined silicon micromachined gratings with a charged-coupled device (CCD) camera and used them in a hybrid system for operation as a spectrometer. More recently, Schmidt et al. (2007) have demonstrated a chip size spectrometer integrated with a microfluidic platform by employing a linear variable band-pass filter and a CMOS camera.

The common issue of the grating-based microspectrometers is their limited spectral resolution, which is typically $R = \lambda/\Delta\lambda = 15$ (Wolffenbuttel 2004), where λ is the nominal wavelength and $\Delta\lambda$ is the minimum detectable change in wavelength. This low resolution results from the short grating-detector distance required for the small system volume. The limited spectral resolution is undesirable for biological assays that require discriminating molecular markers with close spectral characteristics. More importantly, the most dominant factor inhibiting the miniaturization of the entire spectrometer system is the need for highly dedicated computational subunit that runs a spectrum construction algorithm. The highly demanding computational subsystem is often hard to incorporate in the sensing front-end, preventing straightforward sensor integration and miniaturization (Jiao et al. 2003). The heavy computational requirements needed especially for integrating *weak* signals over time result in a slow spectrum acquisition speed (0.01–1 Hz bandwidth), which makes real-time spectroscopy difficult. This obstacle applies to most of fluorophore technology-based biological assays.

Other studies have shown the feasibility of using microfabricated nongrating dispersion elements for infrared (IR) MEMS spectrometer systems. Lammel et al. (2002) developed a tunable reflective filter made out of density modulated porous silicon for analyzing the spectral characteristics of detected light. The transmission spectra of light passing through the filter can be tuned by varying its incident angle. A MEMS thermal actuator is used to turn the filter plate for the wavelength tuning operation. In addition, several thermally tunable bandpass optical filters have been demonstrated, which can be implemented for spectrometer operations (Unamuno et al. 2004; Amano 2003; Yu et al. 2004). These dispersion elements are typically

inexpensive and allow a spectrometer to be operated with only a single detector. However, they inherently suffer from a slow tuning speed as they employ a slow heat transfer process. Manzardo et al. (1999) developed a non-grating MEMS spectrometer based on time-scanning Fourier transform. They fabricated a silicon micromachined Michelson interferometer with a scanning mirror actuated by comb drives. Despite the simplicity of its design and fabrication process, this spectrometer can be only applied for a stationary light source as it requires relatively slow mirror scanning motion at 1 Hz.

With the aim to address the shortcomings of the existing methods described above, we have developed an optical MEMS device, as shown in Figures 1*a*–1*c*

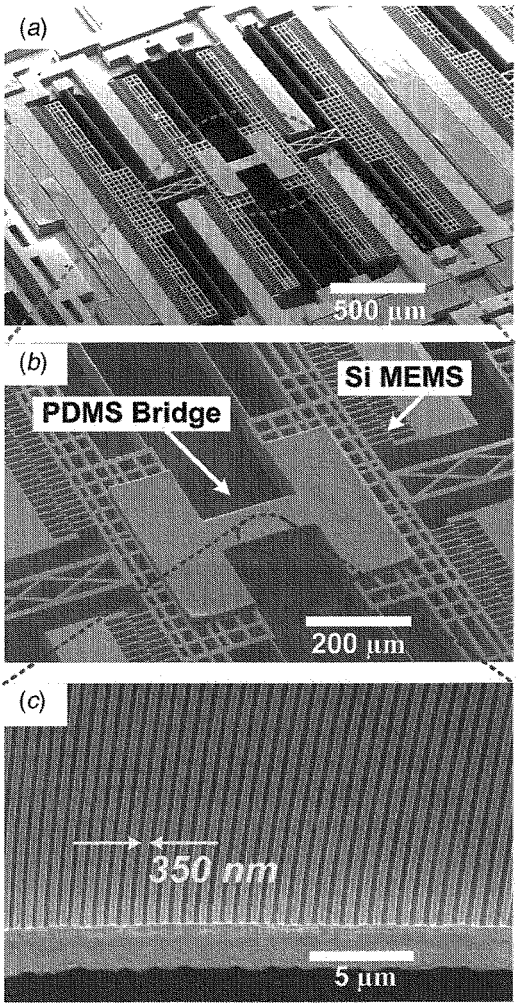

Figure 1. SEM images of the MEMS device. (*a*) The entire device, showing the appositely facing comb drives and the PDMS bridge in the center; (*b*) a closer view of the PDMS microbridge connected to the silicon actuators; and (*c*) a close-up view of the grating pattern on the top surface of the PDMS microbridge. (The color version of this figure can be viewed online at www.informaworld.com.)

(Truxal et al. 2007), which is applicable for high speed, highly sensitive photospectroscopic measurements with a compact system size and can potentially be integrated with a microfluidic system. The device contains electrostatic micro actuators and a tunable polymer diffraction grating made from polydimethylsiloxane (PDMS). A polymer micro-bridge containing a grating pattern with a 700 nm period on the top surface is attached to two oppositely facing silicon comb drives. The optical MEMS device with high-speed wavelength tuning capability is incorporated in a monochromator setup. The monochromator is to have a function that images a single wavelength or a narrow wavelength band onto a photodetector surface and to be used for subsequent spectroscopy experiments. The key advantage of this device is the combination of elastic and silicon structures on the micron scale. The integration of these materials allows the MEMS device to overcome the problems of existing spectrometer setups. The combination of high bandwidth and sufficient tunable range allows the device to be applicable in this monochromator setup, which permits a single point detector with extreme sensitivity. Polymer material also allows for simple mold replication techniques in order to create high groove density gratings without expensive high resolution lithography for fabrication. This article discusses the design of the system to incorporate these advantages of our approach over conventional photospectroscopic techniques.

2. DEVICE OPERATION

2.1. Device Concept

Figure 2*a* illustrates the principle of the device operation. A wavelength scan for incident fluorescence signals is performed by repeatedly varying the PDMS grating pitch with the silicon comb drives driven by an AC actuation voltage signal. The intensity of a particular optical spectrum is detected at a non-space-resolving single detector. Figure 2*b* shows the principle of the device operation for a special case with the incident light normal to the grating plane. A transmission optical grating with a spatial period a lies in the xy-plane, and a light source with a broad wavelength spectrum is incident to the z direction. According to the grating equation, the wavelength of the first order diffraction, λ, observed at a specific angle, θ_1, can be given by $\lambda = a \sin \theta_1$. Through calculations of the period change with strain (see Appendix), it is determined that the wavelength shift of the first order diffraction at the angle θ_1 is linearly proportional to the mechanical strain introduced to the grating structure. Consequently, the peak wavelength of the diffracted light detected at a specific angle can be tuned by controlling the mechanical strain while maintaining the linear strain-diffraction angle relation. It follows that we can obtain plots of emission spectra by mapping the detected intensity and actuation voltage (see Figure 2*c*) by using the force-voltage relation of the MEMS device (see Appendix). This method requires no complicated spectrum-plot construction and signal processing algorithms.

2.2. Device Design for Advantageous Spectroscopy

After evaluating the applications and limitations of current technology described above, we determined targeted specifications of our spectroscopy measurements using the MEMS tunable grating device. The specifications are listed

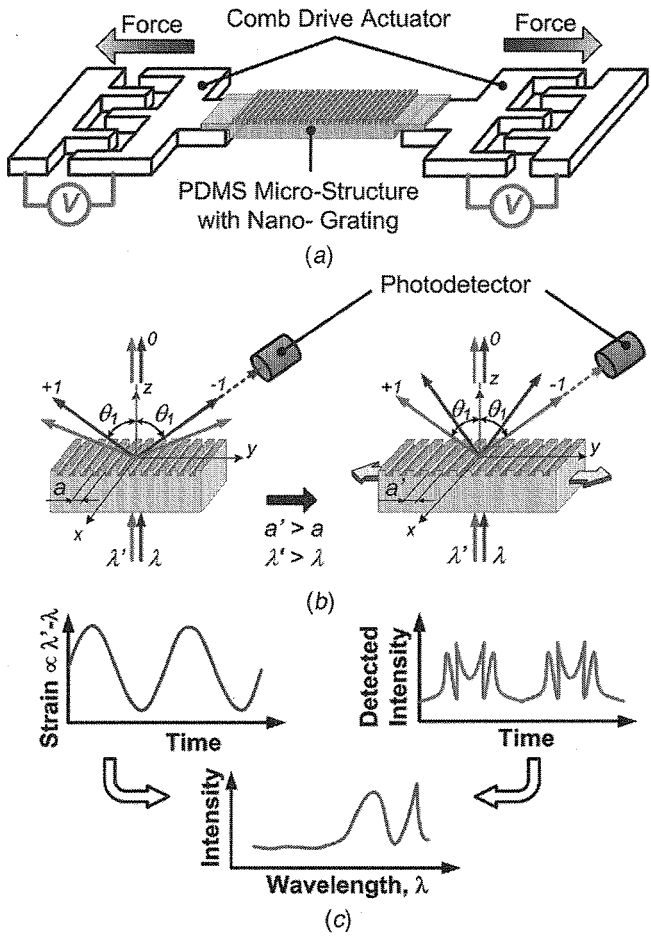

Figure 2. Schematic of strain-tunable nano photonic device with elastomeric nanostructures integrated. (*a*) Device concept, (*b*) operational principle, and (*c*) spectrum data acquisition. (The color version of this figure can be viewed online at www.informaworld.com.)

in the second column of Table 1. Achieving these performance parameters requires careful design of the dimensions, pitch, and shape of the PDMS grating and the comb-drive MEMS structure as described below.

2.2.1. Spectral resolution. One of the most critical grating performance indicators is the spectral resolution as it determines the device's capability of wavelength discrimination. It is defined in terms of "chromatic resolving power" given by $R = \lambda/\Delta\lambda$. The limit of resolution is determined by diffraction theory based on the Rayleigh criterion, which claims that two wavelengths are just resolved when the maximum of one lies at the first minimum of the other. When the dispersed optical spectra are detected at a position far enough to exceed the Rayleigh distance (see Appendix), it is shown $R = mN$ (Born and Wolf 1975), where m is the order of

Table 1 Targeted specifications and current results of spectroscopy measurements.

Spectroscopy specification	Targeted criteria	Current results
Spectral resolution (smallest resolvable wavelength difference)	$\Delta\lambda = 2$–4 nm	$\Delta\lambda = 6$ nm
Wavelength scan range	100–200 nm	65 nm
Grating efficiency	>70%	20%
Dynamic bandwidth	1–5 kHz	1.5 kHz
Actuation voltage	≤150 V	130 V
Optical signal sensitivity @ 1 kHz BW	20–30 pW	36 pW
Power consumption	<7.5 mW	Circuitry dependent

the diffraction, and N is the total number of grating grooves. If we use the first-order mode $m = 1$ that yields the highest intensity for the dispersion operation, our MEMS grating device should yield $R = N = 287$. For the typical visible wavelengths between 450 nm and 650 nm, the theoretical upper bound for $\Delta\lambda$ can be smaller than 2 nm. This preliminary design indicates that the nanometer-scale grating feature is critical for our device to achieve high spectral resolution at this level. The expected value of R for our device is an order of magnitude larger than that of typical MEMS-based micro spectrometers.

2.2.2. Grating efficiency. A high-efficiency grating is often needed for fluorescence spectroscopy that normally requires measuring weak diffracted optical signals. Efficiency is defined as the ratio of the power of monochromatic light diffracted into the order being measured relative to the power of incident light. In general, grating efficiency varies with wavelength as well as with the spectral order and is highly affected by the grating profile. The grating incorporated in our device is a Bragg-condition transmission grating with surface modulated patterns of fine pitch that is comparable to the optical wavelength. Gratings of this type usually deliver high (~90%) first order efficiency almost completely free from polarization effects at a high diffraction angle. The fine grating pitch serves to maintain the high efficiency for a wide wavelength range (Palmer 2002). Previous research (Golub et al. 2004) indicates that the first-order diffraction efficiency of Bragg-condition transmission gratings can be calculated to reach values over 90% (see Appendix). Following this guideline, we can design the profile of the gratings and fabricate the silicon template used in the device processing. The careful grating design process here allows our device to achieve the high efficiency listed in Table 1.

2.2.3. Wavelength scan range. The range of the wavelength achieved for the spectroscopy employing our device is determined by the maximum strain level caused to the PDMS grating structure. To achieve the scan range listed in Table 1, we designed the comb-drive actuators and the PDMS structure such that the maximum strain can be more than 10% under the actuation voltage smaller than 150 V. This is translated into the need for displacement of at least 10 μm generated by comb drives for each end of the PDMS grating structure. The displacement and force generated are directly related to the number of comb finger electrodes, the stiffness of the silicon

suspension beam, and the elasticity of PDMS. We took two approaches to meet the strain requirement. First, we limited the thickness of the PDMS grating structure to less than 5 μm. Due to the softness of PDMS with such small Young's modulus (~750 kPa), achieving the aimed strain level with actuation force smaller than 50 μN is possible. Second, we carefully designed the suspension spring of the comb drives to generate sufficiently large displacement with good stability.

2.2.4. Dynamic response. The speed of the spectrum acquisition is primarily governed by the dynamic bandwidth of our device as the bandwidth of optical detection is typically much larger (>1 MHz). An analytical mass-spring system model can guide our design of the MEMS device. In our preliminary study, we have modeled each of the two silicon comb-drive rotors as moving masses. There are two spring components in the device system: 1) the silicon suspension beam that guides the lateral motion of the rotor and 2) the PDMS grating bridge structure itself. Their spring constants can be calculated using solid mechanics theory. Applying Lagrange's equations to this analytical model allows us to numerically calculate the displacement of the PDMS grating bridge as a function of actuation frequency. Our preliminary calculation indicates that the resonance frequency of the device can be higher than 1 kHz. It follows that the spectrum acquisition can be completed within a millisecond or less.

2.2.5. Optical signal sensitivity. Sufficiently high sensitivity is required for the photodetector coupled with the MEMS grating device to allow for the fast spectrum acquisition mechanism based on "single-shot" optical detection during a single period of the MEMS actuators. For this study we use a photomultiplier tube (PMT) which is capable of very high sensitivity and speeds but has no spatial recognition like the pixilated array of a CCD camera. Optical sensitivity is determined in terms of the minimum detectable power emitted from the sample. In the proposed measurement, 100 different wavelength values need to be evaluated in 1 ms. These values translate to each wavelength value having a 10 μs window in which light is collected from a PMT. The number of counts of photo-induced electrons in the PMT is a function of the light intensity. Based on the PMT (P30CWAD5-01, Electron Tubes Inc., NJ) specifications, we estimate that approximately 10 counts should be accumulated for every 10 μs interval to obtain a signal-to-noise ratio of 10. With the known power needed at the PMT entrance, the power is back calculated to the sample. Assuming an ideal slit and a grating efficiency of 70%, the optical power needed before the grating is approximately 4 pW. The light entering the grating comes from lenses that collect light from the sample. For a sample that emits light in free space equally in all directions, 20% is typically the amount of collected light from an ideal lens. The sample must then be emitting 20 pW of power to adhere to our design specifications for a single period of the MEMS actuators. In our previous flow cytomtery study (Tung et al. 2004), we could successfully detect weak signals from fungus (*S. cerevisiae*) cells labeled by commercial fluorescent markers, such as Syto 62 and Syto 44 (Molecular Probes, OR), using the same level of sensitivity. Therefore, we are confident that the expected sensitivity of our system is large enough for the single-shot rapid spectrum acquisition.

2.3. Device Fabrication

The fabrication of the MEMS device is a multilayer process described in (Tung et al. 2005). The MEMS actuator is fabricated on a silicon-on-insulator (SOI) wafer using standard ultraviolet lithography and deep reactive ion etching. The PDMS structure is created on a separate carrier wafer before being aligned and bonded to the silicon MEMS. The PDMS is cured in a sandwich mold to simultaneously create the bridge shape and nanometer grating pattern through soft lithography. The grating pattern is formed through a nanoimprint of a silicon grating master mold. For the present device the grating master mold is a square pattern with a 700 nm period and 350 nm depth. While the grating pattern efficiency is below 20%, it serves as an excellent base pattern for proving device functionality. Future devices will incorporate a more sophisticated grating master mold for higher grating efficiency without adding any additional fabrication steps.

3. SPECTRAL ACQUISITION

3.1. Measurements of Multi-Wavelength Signal

To demonstrate the spectral acquisition capability of the PDMS-silicon hybrid grating device, we detect two laser light sources with $\lambda = 593$ nm (Rigel-2, Laserglow Technologies) and $\lambda = 633$ nm (25-LHP-991-249, Melles Griot). The optical setup is illustrated in Figure 3. The two lasers are combined using a beam splitter and then directed to pass through the grating. Using a position sensitive diode (PSD) and the red laser, an angle of diffraction of a light signal passing through the PDMS grating was measured for a given actuation voltage. With a sine wave actuation voltage of 0–130 V at 1.5 kHz shown in Figure 4*a*, we obtained a change in angle of approximately 11°, which equates to a grating period strain of 12%. This value of maximum strain agrees well with the predicted calculations of PDMS strain for a given voltage actuation. Slight deviations in the strain profile of the model from the experimental results is likely due to PDMS nonlinearity in straining, and the MEMS silicon beams also acting nonlinear for large displacements. Future research on the material science

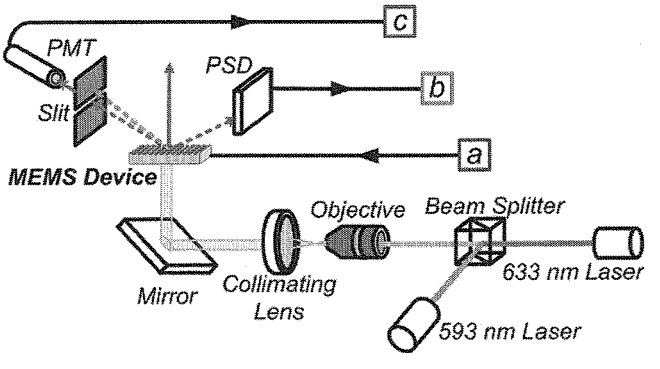

Figure 3. Optical setup for testing device. The input *a* and outputs *b* and *c* correspond to graph (*a*)–(*c*) in Figure 4. (The color version of this figure can be viewed online at www.informaworld.com.)

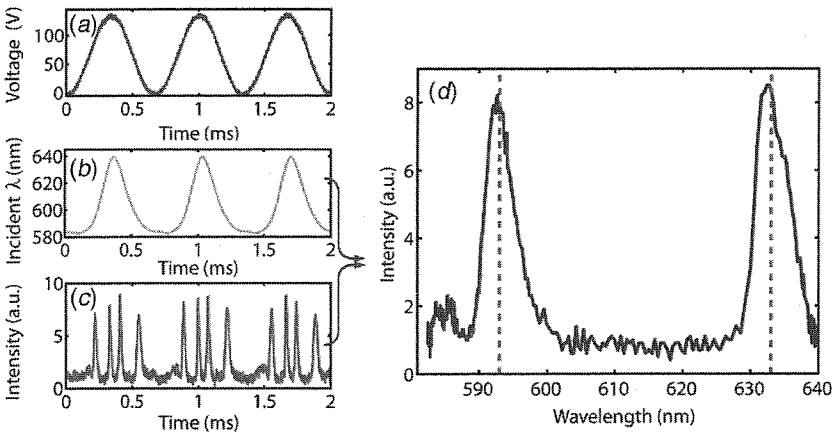

Figure 4. Data results of optical experiments. (*a*) Voltage actuation of the comb drives; (*b*) incident wavelength of the signal onto the photodetector calculated from our characterization of the grating tuning for a given voltage; (*c*) photodiode current measured during simultaneous actuation of the tunable grating; and (*d*) optical spectrum differentiating the mixed wavelength signal that was obtained from spectroscopy employing our MEMS grating device. Dotted lines indicate the actual wavelengths of the detected lasers. (The color version of this figure can be viewed online at www.informaworld.com.)

of PDMS will help build more accurate models of the strain profile. The experimental results, however, can still be used to accurately predict the change in grating with actuation. Using this data, we calculated the incident wavelength onto the photodetector for any applied voltage. With the grating periodicity known for any voltage level, the wavelength incident at the angle of the detector was calculated using the grating equation. The resulting data of the incident wavelength is seen in Figure 4*b*. The photodiode output seen in Figure 4*c* is simultaneously read using a digital oscilloscope during actuation. The two peaks for every half period of actuation correspond to the two first order laser diffractions sweeping over a detector slit. Directly comparing the incident angle data to the photodiode signal creates the spectral differentiation of the light source shown in Figure 4*d*. We can accurately identify the wavelengths and relative intensities within the light signal. Only one full ramp from zero to max actuation voltage (or vice versa) is needed to create the spectroscopic measurements, leading to acquisition times of only 333 μs.

From these measurements we can calculate the spectral resolution. The full-width half-maximum is measured for each peak and set as $\Delta\lambda$ to calculate the resolving power R. The resolving power is approximately 98 for each peak. This value can be improved to the theoretical limit of 287 by adding a focusing element after diffraction and also improving the optical flatness of the grating. Thicker PDMS bridges may improve the optical flatness at the expense of higher actuation forces required. However, the fact that R changes little with actuation is a good indication that the grating is sufficiently flat and consistent with strain. The grating quality may also affect the spectral resolution as well as the grating efficiency. Observations with a scanning electron microscope show that the PDMS grating has very few defects. Ultimately, the quality of the grating and its profile accuracy depend on the master mold grating used for nanoimprinting and soft lithography. A higher quality master

mold for future fabrication will likely increase the resolution of the spectral measurements toward its theoretical limit.

3.2. Measurements of Dynamically Varying Signal

In the next experiment, the detected optical signal is dynamically varied to demonstrate acquisition speed and successive acquisition capabilities. This type of measurement is a good indicator of the device's lab-on-a-chip capabilities, as rapid successive measurements are needed in microfluidics fluorescent detection.

An optical chopper (300CD, Scitec Instruments) is set at 250 Hz and placed in front of the red laser before entering the beam splitter. The red laser signal cycles through being incident onto the grating for 2 ms, then blocked for 2 ms. The yellow laser is kept constant and is always incident onto the grating. Spectral measurements were taken using the same technique described above. The MEMS device is again actuated at 1.5 kHz. A spectral acquisition is taken for every voltage ramp up section of the cycle. The resulting measurement speed is a spectral sweep taken every 667 μs, with a 333 μs acquisition time. While the voltage ramp down section of the cycle can also be analyzed for double the acquisitions, a small pause between measurements may be more appropriate in future applications to differentiate fluorescence samples in microfluidics. Figure 5 displays a series of spectral measurements plotted over time. The plots correctly show the red laser pulsing at 250 Hz while the yellow laser remains constant.

3.3. Long-Term Device Reliability

The repeated cyclic straining of an elastic material does raise concerns over fatigue of the device. Characterization of the mechanical behavior of a similar device

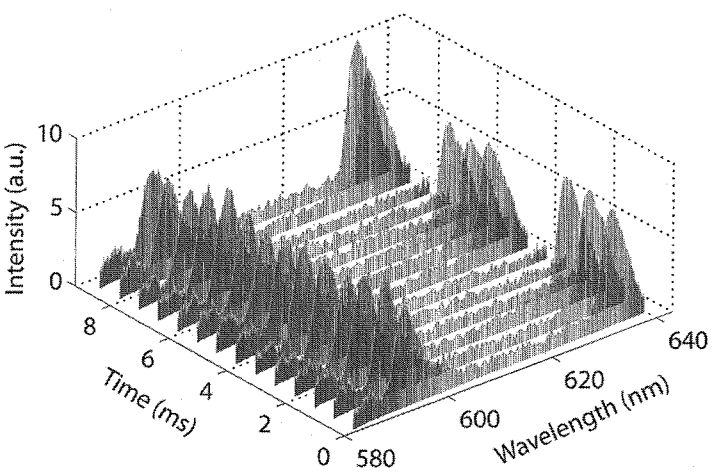

Figure 5. Spectroscopy measurements plotted versus time as the red laser was pulsed at 250 Hz and the yellow laser remained constant. (The color version of this figure can be viewed online at www.informaworld.com.)

has been run and determined that the strain profile does drift slightly over time with continuous actuation. In order to ensure an accurate prediction of the PDMS grating period, cyclic loading measurements using the PSD and a monochromatic source are periodically taken. We have calculated that the cyclic loading measurement taken once every ten minutes of actuation ensures that the spectral measurement accuracy is always within 1 nm. This technique has been very effective in extending the lifetime of devices. Certain devices have seen over 100 million cycles and still yield accurate spectral measurements after characterization.

4. CONCLUSIONS

Our spectroscopic technique only requires a single photodetector through incorporating the strain-tunable MEMS grating device. This has advantages over other methods employing an array of detectors or a pixilated detector such as a CCD camera. This single detector setup allows integration of a highly sensitive detector such as PMT highly suitable for obtaining spectral information in low-intensity fluoroimmunoassays. The setup is simple, power efficient, and maintains sub-millisecond order acquisition speeds. With the application of a PMT, time integration of low intensity spectral signals required from CCD camera spectroscopy is not needed using our technique.

The current device implemented with a single point detector has a limited spectral range of 65 nm due to the microbridge strain induced by the MEMS actuators. This range needs to be expanded to 100–200 nm to meet our original aim to cover a wavelength rage of 400–600 nm, where the spectrum peaks of many important fluorophores lie. In order to increase the range, new devices can be designed to further increase the PDMS strain. Also, another detector could be placed at a different angle at the negative first order to effectively double the range. The maximum sensitivity of similar measurements are also analyzed and discussed elsewhere (Truxal et al. 2008). All of the current device parameters in comparison to our targeted requirements are summarized in Table 1. In order to reach these targets, future designs of the MEMS structure will improve all criteria with none of them yet restricted by any theoretical limits. With the expanded capability, future work will achieve highly sensitive spectrophotometric readings of fluoroimmunoassays at high spectral acquisition speed, with a compact system size.

ACKNOWLEDGEMENTS

This work was supported by National Science Foundation grant No. ECCS-0601237. This research was performed under an appointment to the Department of Homeland Security (DHS) Scholarship and Fellowship Program, administered by the Oak Ridge Institute for Science and Education (ORISE) through an interagency agreement between the U.S. Department of Energy (DOE) and DHS. ORISE is managed by Oak Ridge Associated Universities (ORAU) under DOE contract number DE-AC05-06OR23100. All opinions expressed in this article are the authors and do not necessarily reflect the policies and views of DHS, DOE, or ORAU/ORISE.

REFERENCES

Amano, T. 2003. Design and fabrication of GaAs-GaAlAs micromachined tunable filter with thermal strain control. *Journal of Lightwave Technology* 21(3):596–601.

Born, M. and E. Wolf. 1975. *Principles of optics*. 5th ed. New York: Pergamon.

Goldman, D. S., P. L. White, and N. C. Anheier. 1990. Miniaturized spectrometer employing planar waveguides and grating couplers for chemical analysis. *Applied Optics* 29(31):4583–4589.

Golub, M. A., A. A. Friesem, and L. Eisen. 2004. Bragg properties of efficient surface relief gratings in the resonance domain. *Optics Communications* 235(4–6):261–267.

Jiao, Y., R. Bhalotra, H. L. Kung, and D. A. B. Miller. 2003. Adaptive imaging spectrometer in a time-domain filtering architecture. *Optics Express* 11(17):1960–1965.

Lammel, G., S. Schweizer, S. Schiesser, and P. Renaud. 2002. Tunable optical filter of porous silicon as key component for a MEMS spectrometer. *Journal of Microelectromechanical Systems* 11(6):815–827.

Manzardo, O., H. P. Herzig, C. R. Marxer, and N. F. de Rooij. 1999. Miniaturized time-scanning fourier transform spectrometer based on silicon technology. *Optics Letters* 24:1705–1707.

Mohr, J., B. Anderer, and W. Ehrfeld. 1991. Fabrication of a planar grating spectrograph by deep-etch lithography with synchrotron radiation. *Sensors and Actuators A: Physical* 27(1–3):571–575.

Palmer, C. 2002. *Diffraction grating handbook*. 5th ed. Rochester, NY: Spectra Physics.

Sander, D. and J. Muller. 2001. Self-focusing phase transmission grating for an integrated optical spectrometer. *Sensors and Actuators A: Physical* 88(1):1–9.

Schmidt, O., M. Bassler, P. Kiesel, C. Knollenberg, and N. Johnson. 2007. Fluorescence spectrometer-on-a-fluidic-chip. *Lab Chip* 7(5):626–629.

Truxal, S. C., Y.-C. Tung, and K. Kurabayashi. 2007. A PDMS-on-silicon deformable grating for spectral differentiation of mixed wavelength signals. *Proc. Transducers & Eurosensors '07* 1:1087–1090.

Truxal, S. C., Y.-C. Tung, and K. Kurabayashi. 2008. High-speed deformation of soft lithographic nanograting patterns for ultrasensitive optical spectroscopy. *Applied Physics Letters* 92(5):051116-1-3.

Tung, Y. C., M. Zhang, C. T. Lin, K. Kurabayashi, and S. J. Skerlos. 2004. PDMS-based opto-fluidic micro flow cytometer with two-color, multi-angle fluorescence detection capability using PIN photodiodes. *Sensors and Actuators B: Chemical* 98(2–3):356–367.

Tung, Y.-C., S. C. Truxal, and K. Kurabayashi. 2005. Multi-scale soft-lithographic lift-off and grafting (MS-SLLOG) process for active polymer nanophotonic device fabrication. *Proceedings of SPIE - The International Society for Optical Engineering* 6050:605002-1-10.

Unamuno, A., L. Li, and D. Uttamchandani. 2004. Fiber Bragg grating demodulator based on hybrid optical MEMS. *IEEE Journal of Selected Topics in Quantum Electronics* 10(3):598–603.

Wolffenbuttel, R. F. 2004. State-of-the-art in integrated optical microspectrometers. *IEEE Transactions on Instrumentation and Measurement* 53(1):197–202.

Yee, G. M., N. I. Maluf, P. A. Hing, M. Albin, and G. T. A. Kovacs. 1997. Miniature spectrometers for biochemical analysis. *Sensors and Actuators A: Physical* 58(1):61–66.

Yu, B., G. Pickrell, and A. Wang. 2004. Thermally tunable extrinsic Fabry-Perot filter. *IEEE Photonics Technology Letters* 16(10):2296–2298.

APPENDIX

Strain-Wavelength Shift Relationship

When introducing a mechanical strain to elongate the spatial period of the grating to a', the wavelength of the first order diffraction at the same angle θ_1 shifts to λ'. The corresponding mechanical strain ε can be defined as

$$\varepsilon = \frac{a' - a}{a} = \frac{a'}{a} - 1 \tag{1}$$

Then, the relation between the wavelength shift $\lambda' - \lambda$ and the mechanical strain can be given by

$$\lambda' - \lambda = a\varepsilon \sin\theta_1 = \lambda\varepsilon \tag{2}$$

Force-Voltage Relationship

The MEMS device creates mechanical force for a given applied actuation voltage difference. This force is also proportional to the wavelength shift through the mechanical strain given by

$$\lambda' - \lambda \propto \varepsilon \propto F = \frac{\varepsilon_0 t N_g V^2}{2g} \tag{3}$$

where t is the in-depth thickness of the comb drive, N_g is the total number of gaps, g is the gap between the comb electrodes, ε_o is the permittivity of free space, and V is the actuation voltage.

Ideal Grating Efficiency

The grating efficiency for a Bragg-condition transmission grating is given by

$$\eta_1 = \sin^2\left(\sqrt{\nu_1^2 + \xi_1^2}\right)\left[1 + (\xi_1\nu_1)^2\right]^{-1} \tag{4}$$

where the non-dimensional parameters ν_1 and ξ_1 are determined by the grating groove depth, the grating period, the refractive index of the grating material, and the incident angle. Based on a model approximating the grating profile to be sinusoidal, our preliminary calculation predicts very high efficiency above 90% when the aspect ratio of the grating groove becomes nearly 2 for the index of PDMS $\sim$1.45.

Rayleigh Distance

The Rayleigh distance is given by

$$D = N^2 a^2/\lambda \tag{5}$$

which is approximately 6.3 cm for a grating with $a = 700$ nm and a length of 200 μm. This calculation ensures that we can still use the far-field diffraction theory for our grating design while we assume the entire device size is sufficiently compact.